Dalton Transactions

Accepted Manuscript

This article can be cited before page numbers have been issued, to do this please use: M. Harris, C. Henoumont, W. Peeters, S. Toyouchi, L. Vander Elst and T. Parac-Vogt, *Dalton Trans.*, 2018, DOI: 10.1039/C8DT01227J.

ROYAL SOCIETY OF CHEMISTRY

rsc.li/dalton

View Article Online
DOI: 10.1039/C8DT01227J

Journal Name

ARTICLE

Amphiphilic complexes of Ho(III), Dy(III), Tb(III) and Eu(III) for optical and high field magnetic resonance imaging †

Received 00th January 20xx,
Accepted 00th January 20xx

DOI: 10.1039/x0xx00000x

www.rsc.org/

Michael Harris,[a] Céline Henoumont,[b] Wannes Peeters,[a] Shuichi Toyouchi,[a] Luce Vander Elst,[b] and Tatjana N. Parac-Vogt[a]*

Lanthanides holmium(III), dysprosium(III), and terbium(III) were coordinated to an amphiphilic DOTA *bis*-coumarin derivative and then further assembled with an amphiphilic europium(III) DTPA *bis*-coumarin derivative into mono-disperse micelles. The self-assembled micelles were characterized and assessed for their potential as bimodal contrast agents for high field magnetic resonance and optical imaging applications. All micelles showed high transverse relaxation (r_2) of 46, 34, and 30 s^{-1} mM^{-1} at 500 MHz and 37 °C for Dy(III), Ho(III) and Tb(III) respectively, which is a results of the high magnetic moment of these lanthanides and long rotational correlation time of the micelles. The quantum yield in aqueous solution ranged from 1.8% for Tb/Eu to 1.4% for Dy/Eu and 1.0% for the Ho/Eu miceles. Multi-photon excited emission spectroscopy has shown that due to two-photon absorption of coumarin chromophore the characteristic Eu(III) emission could be observed upon excitation at 800 nm, demonstrating the usefulness of the system for *in vivo* fluorescence imaging applications. To the best of our knowledge this is the first example reporting the potential of a holmium(III) chelate as a negative MRI contrast agent.

Introduction

Magnetic resonance imaging (MRI) is a powerful *in vivo* technique used in clinical diagnostics. The main advantage of MRI is that there is no ionizing radiation used for acquiring whole body, three-dimensional images, unlike positron emission tomography (PET) or X-ray imaging. However, despite the good spatial resolution of MRI, this technique suffers from intrinsically low sensitivity, and thus often high concentrations of contrast agents (CAs) are required.[1] Recently the research in the area of contrast agent bimodality has gained increasing interest as it couples MRI with other diagnostic techniques endowed with high sensitivity.[2-5] PET/MRI scanners have already found clinical application but MRI/optical imaging is still lagging behind due to limitations imposed by the optical transparency of biological tissues.[6] Currently, the bimodal MRI/optical imaging technique is being investigated in small animal models due to the closer proximity of organs to the body surface.[7] Ideally the near-infrared (NIR) window (650 to 1350 nm) is the focus of research into emissive probes for this application due to the maximum depth penetration at these wavelengths.[8]

The most commonly used contrast agents for MRI include gadolinium(III) chelates of diethylenetriaminepentaacetic acid (DTPA) and 1,4,7,10-tetraazacyclododecane-1,4,7,10-tetraacetic acid (DOTA). Gadolinium(III) is endowed with several favourable properties required for CAs such as a large number of unpaired electrons and a long electronic relaxation time. Despite gadolinium(III) chelates being the 'gold standard' of CAs, their performance is only well suited for current MRI scanners which typically operate at 60 MHz.[1] Contrast enhancement of these CAs drops dramatically from 1 to 100 MHz, with an r_1 of ~3-4 s^{-1} mM^{-1} reported at 60 MHz and 37 °C.[1] Increasing the strength of magnets towards higher magnetic fields in the MRI diagnostic instruments is an alternative for enhancing the sensitivity of this technique which renders gadolinium(III) chelates rather obsolete as positive CAs in the future.[9]

Various nanoparticles (NPs) and molecular complexes have been investigated as potential bimodal MRI/optical probes.[10-14] For example paramagnetic iron oxide NPs decorated with fluorescent probes have been shown to act as negative MRI CAs which also have interesting optical properties.[15-20] Upconverting and paramagnetic NPs have been also reported as bimodal CAs.[21, 22] These NPs can be excited with long wavelength lasers and show impressive relaxation properties; however, cytotoxicity of these NPs has yet to be evaluated.

In addition to NPs, increasing the rotational correlation time of lanthanide(III) chelates by conjugation to macromolecules, such as polymers and dendrimers,[23-26] or

[a] KU Leuven, Department of Chemistry, Celestijnenlaan 200F, 3001 Leuven, Belgium. E-mail: tatjana.vogt@kuleuven.be
[b] General, Organic and Biomedical Chemistry, NMR and Molecular Imaging Laboratory, University of Mons, 7000 Mons, Belgium.
†Electronic Supplementary Information (ESI) available.
See DOI: 10.1039/x0xx00000x

View Article Online
DOI: 10.1039/C8DT01227J

supramolecular assembly into micelles and liposomes can significantly increase the CAs relaxation performance.[27-31] Lanthanide systems overcome the drawbacks of organic dyes such as short fluorescence lifetimes, small Stokes' shifts, and photobleaching. Moreover, lanthanide(III) ions with large magnetic moments such as terbium ($9.8\mu_B$), dysprosium ($10.6\mu_B$) and holmium ($10.7\mu_B$) should display efficient transverse relaxivity at strong magnetic fields, making them suitable for designing negative T_2 contrast agents for MRI. The effect of increased field strength on transverse relaxation rate (r_2) is even more pronounced in complexes with large rotational correlation times (τ_r).[32] One of the ways to achieve the increase in τ_r of lanthanide complexes is by incorporating them into larger systems such as micelles or liposomes.[33-35]

We have previously investigated Tb(III) and Dy(III) micellar chelates as single lanthanide bimodal CAs for MRI and optical imaging.[27, 29-31] Despite their impressive performance as T_2 contrast agents at high magnetic fields, the drawback of these systems was the short excitation wavelength used to observe luminescence signal (< 300 nm), which restricts their potential in biological applications.[27, 29-31] In order to circumvent this problem, in this work we designed a binary system in which an Eu(III) complex is used as an optical probe, and a complex based on an Ln(III) ion with high magnetic moment acts as T_2 contrast agent. We envisioned that incorporation of such complexes into a single micelle will result into a nano-aggregate system with a large rotational correlation time and favourable magnetofluorescent properties. In addition to Tb(III) and Dy(III) complexes, which were previously demonstrated to act as T_2 contrast agents,[27, 29-31] in this work we also examine complexes based on Ho(III). Despite the fact that Ho(III) has the largest magnetic moment (10.7 μB) among all the lanthanides the potential of its complexes as negative contrast agents has been virtually unexplored and the focus has been largely on ^{166}Ho as a radionuclide.[36] Few recent studies reported on the potential of Ho_2O_3 and metal organic framework based nanoparticles as a MRI contrast nanoprobe,[37-40] however, to the best of our knowledge, chelate complexes based on Ho(III) have been virtually unexplored as high field T_2 contrast agents.

Results and discussion

Synthesis of ligands, complexes and micelles

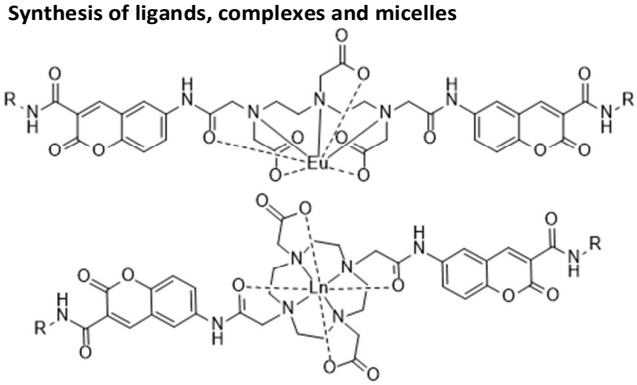

Figure 1. Eu(III)-DTPA-BC_{10}coumarin (upper), Ln(III)-DOTA-BC_{10}coumarin (lower). Ln represents Tb, Dy, Ho and R = *n*-$C_{10}H_{21}$. The coordinated water molecule is omitted.

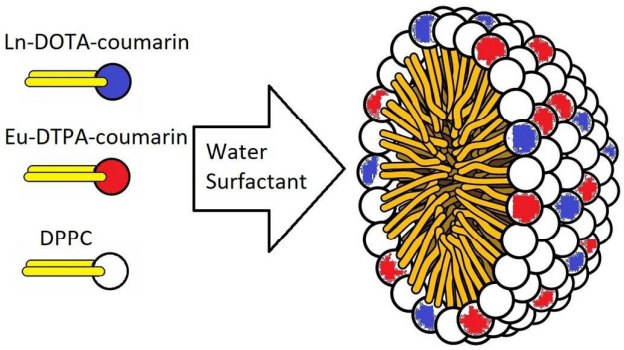

Figure 2. Schematic of the mixed micelles. Eu-DTPA-BC_{10}coumarin (red), Ln(III)-DOTA-BC_{10}coumarin (blue), and DPPC (white). Surfactant Tween 80® is omitted.

The optical probe was designed by using a coumarin chromophore due to its efficient energy transfer to Eu(III), and its potential to undergo multi-photon excited emission at 800 nm. [41] Sensitized Eu(III) ions emit red light with the most interesting emission line for this application being centred around 700 nm and a long luminescence lifetime in the millisecond range.[42]

Synthesis of the coumarin derivative bearing an alkyl chain and connection to DTPA *bis*-anhydride was performed following procedure developed by our group.[43] Similarly, the reduced coumarin was reacted with chloroacetyl chloride and connected to a DOTA derivative which had been pre-functionalized in a *trans*-fashion with tertiary butyl acetate groups by modifying a reported procedure.[29, 31] The ligands have been characterised by nuclear magnetic resonance spectroscopy, mass spectrometry, and IR spectroscopy.

The DTPA chelator was coordinated to europium(III) and DOTA chelator to terbium(III), dysprosium(III) and holmium(III) in pyridine according to a literature procedure (Figure 1). The presence of coumarin in DOTA ligand is also beneficial from the relaxivity point of view as it contains a fused 2-ring system that makes it a rigid molecule. The rigid ligand environment is expected to reduce the local motions of the Ln(III) ion and result in enhanced relaxivity.[1] The absence of free lanthanide(III) ions was verified with an arsenazo indicator solution.[44] Mass spectrometry and IR spectroscopy were used to confirm the complex formation.

Molecular design of the complexes bearing hydrophobic alkyl chains and a hydrophilic head-group allows facile incorporation into mixed micelles with DPPC and supporting surfactant Tween 80® (Figure 2). Self-assembly of Ln(III) complexes into such large nano-aggregates is expected to further limit the local motions of the complexes and to result in increase of the rotational correlation time. Micelles were produced by mixing 1 equivalent of Ln(III)-DOTA chelate acting as MRI probe, 1 equivalent of Eu(III)-DTPA-BC_{10}coumarin as optical probe, 12 equivalents of phospholipid (DPPC), and 6.5 equivalents of surfactant (Tween 80®). For the sake of simplicity in this proof-of-concept design, we have chosen a ratio of 1:1 for MRI to optical probe, but this ratio could be varied and optimized for any application based on the emission intensity needed of Eu(III). Dynamic light scattering measurements confirmed formation of the mono-disperse micelles with particle distribution maxima of ~25 nm (Supporting Information, Figure S1 and S2). This value is in good agreement with the study of Lim *et al* who have

View Article Online
DOI: 10.1039/C8DT01227J

performed detailed characterisation of DPPC/Tween 80® micelles, which were found to have similar radius as the ones reported in this work.[45] Such micelle systems appear to be very stable in aqueous solution, as previously confirmed by DLS[31] and intermolecular energy transfer experiments.[43]

Photophysical properties of lanthanide nanoaggregates

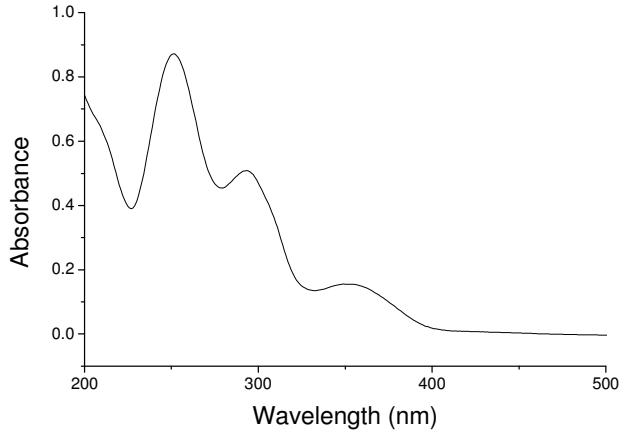

Figure 3. Absorbance spectrum of Eu(III)-DTPA-BC_{10}coumarin micelles in water (0.1 wt%, 298 K).

The Eu(III)-DTPA-BC_{10}coumarin derivative assembled into micelles shows multiple well-defined absorbance bands in the 200 to 400 nm region of spectrum (Figure 3). Interestingly, Eu(III) coordinated to coumarin-DOTA chelator showed very poor energy transfer when aggregated into micelles and therefore it was necessary to use DTPA as the chelator for the optical probe, despite lower kinetic stability of such complexes compared to DOTA chelator. We speculate that this could be due to the orientation of the coumarin chromophore being unsuitable for efficient energy transfer to the Eu(III) ion. The excitation spectra (Figure 4) of micelles incorporating both Ln(III)-DOTA-BC_{10}coumarin (Ln = Ho, Dy, Tb) and Eu(III)-DTPA-BC_{10}coumarin complexes show a broad excitation peak from 230 nm to ca. 425 nm, with the most efficient excitation at 350 nm, and with no significant variation based on the nature of Ln(III) ion. All emission spectra display the sharp emission bands of the Eu(III) ion which are attributed to the $^5D_0 \rightarrow {}^7F_J$ (J = 0-4) transitions.

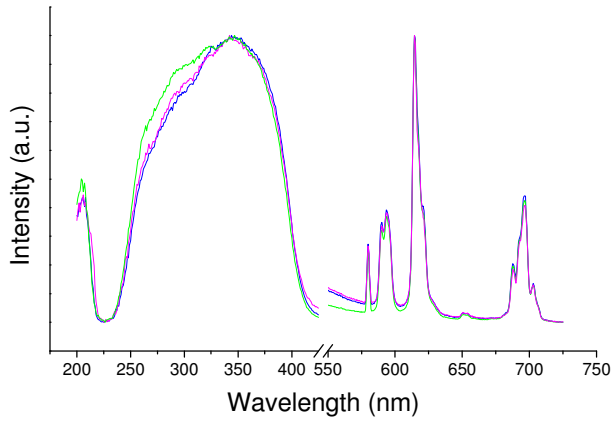

Figure 4. Normalised excitation and emission spectra of Ln(III)-DOTA-/Eu(III)-DTPA-BC_{10}coumarin micelles in water (0.1 wt%, 298 K, Exc 350 nm, Emi 615 nm), Tb(III) (green), Dy(III) (blue), Ho(III) (magenta).

Luminescence lifetimes in H_2O and D_2O have been obtained by fitting mono-exponential equations to the luminescence decays of Eu(III) (table 1). Two equations developed for cyclen[46] and aminocarboxylate derivatives[47] allow the number of coordinated water molecules q to be calculated with an accuracy of ± 0.2-0.3 for equation (1) and ± 0.1 for equation (2):

$$q_{\mathrm{Eu}}(\mathrm{H_2O}) = 1.2(\Delta k_{obs} - 0.25 - 1.2q^{\mathrm{NH}} - 0.075q^{\mathrm{CONH}}) \quad (1)$$

$$q_{\mathrm{Eu}}(\mathrm{H_2O}) = 1.11(\Delta k_{obs} - 0.31 - 0.44q^{\mathrm{OH}} - 0.99q^{\mathrm{NH}} - 0.075q^{\mathrm{CONH}}) \quad (2)$$

In the equations above $\Delta \boldsymbol{k_{obs}}$ represents the difference in the decay rate constants $\Delta \boldsymbol{k_{H_2O}}(\boldsymbol{1/\tau_{H_2O}})$ and $\Delta \boldsymbol{k_{D_2O}}(\boldsymbol{1/\tau_{D_2O}})$ and q^{X} stands for the number of OH, NH or CONH groups participating in lanthanide coordination. In the Eu(III)-DTPA-BC_{10}coumarin complex, only amide groups are considered, resulting in q_{Eu} values of 0.6 to 0.8 according to Eq 1 and 2 respectively. Although it is expected that there should be one coordinated water molecule in the ninth vacant coordination site of the Eu-complex, it has been often observed that in similar micelle systems the surfactant competes for lanthanide coordination resulting in values lower than 1. The quantum yields have been determined for all three micelle systems, reaching 1.8% for the Tb/Eu combination but dropping to 1.4% and 1% for the Dy/Eu and Ho/Eu systems respectively.

Table 1. Photophysical data for the Ln(III)/Eu(III) micelles in water (0.1 wt%) at 298 K.

Complex	τ H_2O^a [ms]	τ D_2O^a [ms]	q H_2O [Eu]	$Q_{Ln}^{L}{}^b$ [%]
Tb/Eu	0.63	1.7	$0.8^c/0.7^d$	1.8
Dy/Eu	0.53	1.2	$0.7^c/0.6^d$	1.4
Ho/Eu	0.49	1.1	$0.8^c/0.7^d$	1.0

[a] Average of three measurements which vary by no more than 0.2 µs.
[b] Estimated relative errors $\boldsymbol{Q_{Ln}^{L}}$ ± 10%. Quantum yields relative to rhodamine 101 in ethanol.
[c] equation 1. [d] equation 2.

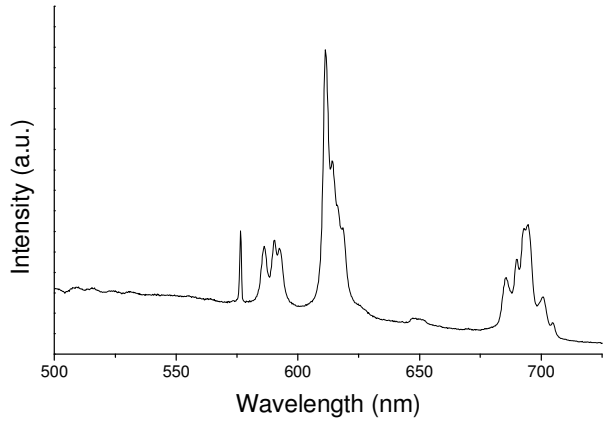

Figure 5. 2PE spectra of Eu(III)-DTPA-BC_{10}coumarin micelles in water (800 nm Ti:sapphire laser excitation, 0.1 wt%, 298 K).

View Article Online
DOI: 10.1039/C8DT01227J

The excitation wavelength of 350 to 425 nm that was used to observe Eu(III) luminescence shown in Figure 4 is generally compatible for *in vitro* cellular imaging due to commercially available laser wavelengths of 355 and 405 nm for fluorescence confocal microscopy. Indeed, we have previously shown that in related Eu(III)-DTPA-BC_{10}coumarin complexes, it was possible to observe Eu(III) emission by using a 405 nm laser.[43] On the other hand two-photon excited emission (2PE) is of particular interest for *in vitro* studies due to the enhanced depth discrimination, and also for *in vivo* studies due to the reduction of photo-damage and increased optical transparency of living tissues to light in the 650 to 1350 nm range.[48, 49]

The ability of Eu(III)-DTPA-BC_{10}coumarin to act as optical probe in biologically relevant spectral range was evaluated by using two-photon excited emission (2PE) spectroscopy. Figure 5 shows the 2PE spectrum that was observed using an excitation wavelength of 800 nm (Ti:sapphire laser). The results indicate that the coumarin chromophore is able to absorb two photons of 800 nm and transfer energy to the Eu(III) ion at a higher wavelength of approx. 400 nm. The emission lines are identical to the single photon spectrum, and can be attributed to the $^5D_0 \rightarrow {}^7F_J$ (J = 0-4) transitions. Among these characteristic Eu(III) emission lines, the most relevant emission for biomedical optical imaging is the one centred around 690 nm as it falls within the NIR window (650 to 1350 nm).[8]

Relaxometric studies of lanthanide nanoaggregates

Proton longitudinal relaxation rate

The enhancement of water relaxation rate by 1 mM of each Ln(III) complex determines its proton longitudinal relaxivity, r_1. Figure 6 shows the r_1 values of the 3 different Ln(III)-micelle systems at 20, 60, 300, and 500 MHz. All of the 3 systems follow the same trend, in which at lower magnetic fields (20 – 60 MHz), low r_1 values or 0.18 – 0.24 s^{-1} mM^{-1} are observed while at high magnetic fields (300 – 500 MHz,) an increase in relaxivity is observed. The largest increase was observed for Dy(III)/Eu(III) micelles, followed by Ho(III))/Eu(III) and Tb(III))/Eu(III) micelles. Inner- ($\mathbf{1}/\boldsymbol{T_1^{is}}$) and outer-sphere ($\mathbf{1}/\boldsymbol{T_1^{os}}$) contributions to the proton longitudinal relaxation rate are defined by the sum of dipolar ($\mathbf{1}/\boldsymbol{T_1^{DD}}$) and Curie ($\mathbf{1}/\boldsymbol{T_1^{C}}$) contributions. At low magnetic fields, the electronic relaxation time, τ_S, contributes mostly to the longitudinal relaxation rate, which is modulated through the dipolar interactions between the water proton nuclei and the static magnetic moment of the electrons of the Ln(III) ions. The very short τ_S for these heavier lanthanides explains the low r_1 values in comparison to Gd(III) which possesses a τ_S of around 2 orders of magnitude greater (~100 vs ~0.5 ps).[28] An increase is observed at higher magnetic fields due to the Curie inner- and outer-sphere contributions becoming more significant. These terms are modulated by the rotational correlation time of the compound τ_R and the translational correlation time τ_D; τ_D equals a^2/D, in which a is the distance of the closest approach between the water protons and the paramagnetic centre, and D is the relative diffusion constant of the water molecules and the complex. Fitting of the r_1 data allowed an estimate of the τ_S and τ_R values (table 2). During the fitting procedure, the parameters r = 0.31 nm, a = 0.36 nm and D = 3.0 x 10^{-9} m^2 s^{-1} were fixed (Solomon-Bloembergen-Morgan theory).[50-52] The value of q is generally obtained from the luminescence lifetimes of the lanthanide complexes. However, in the case of DOTA-BC_{10}coumarin complexes of Dy(III) and Tb(III), the energy transfer from coumarin to the lanthanides was not observed, while aqueous luminescence of Ho(III) is considered to be very rare.[53] Due to Eu(III) being coordinated to a slightly different DTPA vs DOTA chelator, we have not used the values obtained from those lifetimes measurements. Instead the q value was fixed to 1, as the 8 coordinate DOTA would have 1 vacant coordination place available for water. In addition, DOTA complexes have been reported to have slightly higher q values than their DTPA analogues.[27, 29-31]

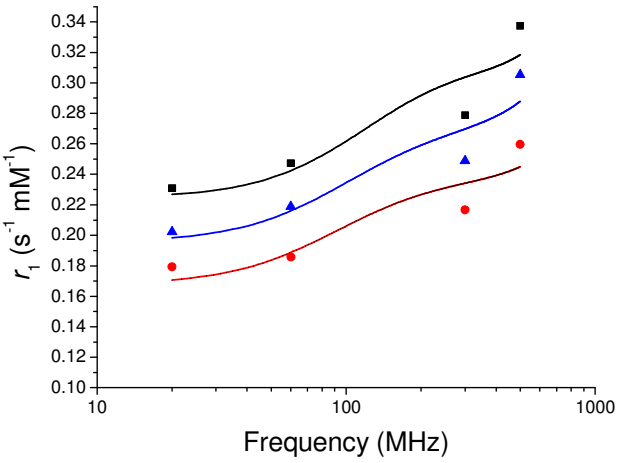

Figure 6. Proton longitudinal relaxivity of the micelles versus proton Larmor frequency. Tb(III)/Eu(III) (red), Ho(III)/Eu(III) (blue), and Dy(III)/Eu(III) (black). The lines represent the fitted data.

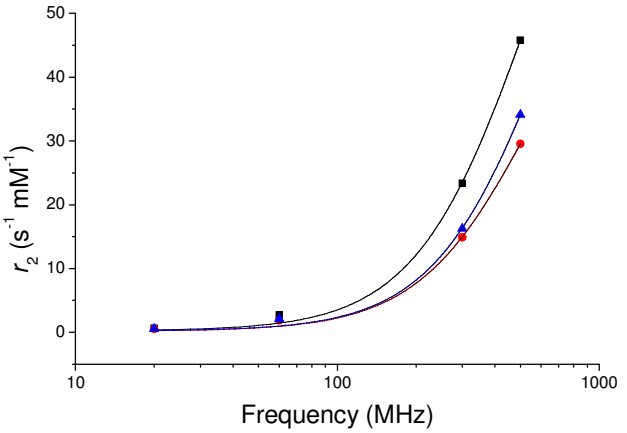

Figure 7. Proton transverse relaxivity of the micelles versus proton Larmor frequency. Tb(III)/Eu(III) (red), Ho(III)/Eu(III) (blue), and Dy(III)/Eu(III) (black). The lines represent the fitted data.

Proton transverse relaxation rate

The T_2 enhancements at 20, 60, 300, and 500 MHz by the Ln(III)/Eu(III) micelles are shown in Figure 7. At low frequency (20 – 60 MHz), the transverse relaxivities are slightly higher than the longitudinal values (r_1 ~0.2 vs r_2 ~0.55) due to the aggregation of the complexes in micelles. Most significant to these micelle systems

View Article Online
DOI: 10.1039/C8DT01227J

is the increase in r_2 which takes place at higher magnetic fields (ν_o > 100 MHz). Despite transverse relaxivity increasing proportionally to the square of the magnetic field, a much larger increase than this alone was observed. The added enhancement in r_2 is the strong reliance to the τ_M value with increasing external magnetic field. In order to achieve this strong influence on r_2, is important that the chemical shift difference between coordinated and bulk water ($\Delta\omega_M$) remains low relative to the water exchange in order to avoid the limitation by τ_M.[54] The chemical shift of the coordinated water molecule is proportional to the magnetic field and is the sum of contact and pseudocontact terms.

Fitting of the data is performed using the equations defining the inner- and outer-sphere contributions as described by Vander Elst *et al*.[54] The inner-sphere contributions depend on the [Ln(III) complex/[water], the *q* value, water residence time τ_M and the transverse relaxation rate of the coordinated water molecule, $1/T_{2M}$. The last factor results from dipolar, dipolar Curie, and Curie contact contributions.

The correlation time τ_C modulating the dipolar interaction is related to τ_R, τ_S, and τ_M through $\tau_C^{-1} = \tau_R^{-1} + \tau_S^{-1} + \tau_M^{-1}$ whereas the Curie contribution is modulated by $\tau_{CC}^{-1} = \tau_R^{-1} + \tau_M^{-1}$. Paramagnetic relaxation theory takes into consideration the distance between the water protons and the paramagnetic centre (r), and the residence time of coordinated water molecules (τ_M). The parameters τ_M and $\Delta\omega_M$ were obtained from the fittings of r_2 data and are listed in Table 2. However, they should be considered as estimates as the fit is only over four points for r_1 and r_2.

Table 2. Values of τ_S, τ_R, τ_M, and $\Delta\omega_M$ obtained by fitting of the ^{1}H $r_{1,2}$ data of the micelles at 310 K.

Complex	τ_S (ps)	τ_R(ns)	τ_M (ns)	$\Delta\omega_M$ (10^5 rad s^{-1} T^{-1})
Tb/Eu	0.29±0.02	1.7±0.4	266±38	2.8±0.1
Dy/Eu	0.35±0.02	1.3±0.3	180±20	4.3±0.1
Ho/Eu	0.30±0.03	1.6±0.4	197±37	3.3±0.2

Table 2 shows that the most significant difference among three examined micelle systems is the water residence time (τ_M), which was determined to be 266, 180, and 197 ns for Tb(III), Dy(III) and Ho(III) respectively. The values for Tb(III) and Dy(III) are in the same range as those reported before for similar DOTA micelle systems,[29, 31] however, no previous reference for Ho(III)'s water residence time in DTPA or DOTA complexes could be found in literature. One of the plausible explanations for the observed variation in τ_M is the decreasing ionic radius of the lanthanide(III) ions. As the chelator becomes more 'crowded' around the Ln(III) ion it affects the water coordination, and this along with the difference in magnetic moments and electronic relaxation times of the Ln(III) ions leads to the observed results. It has been reported that increasing the water residence time (from 0.1 to 1 µs) for Dy(III)-DTPA complexes with the same electronic relaxation times will increase the transverse relaxation performance.[54] The electronic relaxation times from our fitting procedure are in agreement with a study by Bertini *et al.* of the un-chelated Ln(III) aqua ions, which reported values of τ_S = 0.38 and 0.27 ps for Dy(III) and Ho(III) respectively at 308 K.[55] Among the examined lanthanides(III) micelles in this study, those based on Dy(III) appear to be the most efficient towards the increase of the transverse relaxation rate due to an optimal combination of its intermediate τ_M and its slightly higher value of τ_S compared to Ho(III) and Tb(III) ions.

Conclusions

A series of binary systems based on of amphiphilic Ln(III)/Eu(III) complexes was investigated and showed favourable magnetic and optical properties, including the first example of a Ho(III)-chelate as a T_2 contrast agent. The micelles showed impressive transverse relaxation resulting from the large magnetic moments of the Ln(III) ions and increased rotational correlation time of the micelles. The optical probe based on Eu(III)-DTPA-coumarin exhibits a long luminescence lifetime and a relatively large quantum yield in aqueous solution. Multi-photon excited emission spectroscopy in the NIR region have shown that the Eu(III) optical probe could be useful for the potential *in vivo* fluorescence imaging applications. Moreover, a modular design allows the optical probe to be included at any ratio depending on particular application. Among the series of lanthanides(III) chelates that possess large magnetic moments dysprosium(III) performs the best as a MRI transverse relaxation contrast agent due to optimal combination of its electronic relaxation and water residence times.

Conflicts of interest

There are no conflicts to declare.

Acknowledgements

M. H. would like to acknowledge the Research Foundation Flanders (F.W.O) for a PhD scholarship. M.H. and T.P.V. thank Prof. Dr. Jef Rozenski for accurate mass measurements, Laboratory of Medicinal Chemistry, Rega Institute, KU Leuven. Mass spectrometry was made possible by the support of the Hercules Foundation of the Flemish Government (grant 20100225–7).

Experimental

Materials

Reagents and solvents were obtained from Sigma–Aldrich (Bornem, Belgium), Acros Organics (Geel, Belgium), ChemLab (Zedelgem, Belgium), Matrix Scientific (Columbia, USA) and BDH Prolabo (Leuven, Belgium), and were used without further purification. Europium(III) chloride hexahydrate was obtained from Sigma–Aldrich (Bornem, Belgium).

Instrumentation

^{1}H spectra were recorded by using a Bruker Avance 300 spectrometer (Bruker, Karlsruhe, Germany), operating at 300 MHz for ^{1}H.

IR spectra were measured by using a Bruker Vertex 70 FT-IR spectrometer (Bruker, Ettlingen, Germany).

View Article Online
DOI: 10.1039/C8DT01227J

ESI-Mass spectra were obtained by using a Thermo Finnigan LCQ Advantage mass spectrometer. Samples for the mass spectrometry were prepared by dissolving the product (2 mg) in methanol (1 mL), then adding 200 µL of this solution to a water/methanol mixture (50:50, 800 µL). The resulting solution was injected at a flow rate of 5 µL min^{-1}.

Accurate mass spectra were acquired on a quadrupole orthogonal acceleration time-of-flight mass spectrometer (Synapt G2 HDMS, Waters, Milford, MA). Samples were infused at 3uL/min and spectra were obtained in positive ionization mode with a resolution of 15000 (FWHM) using leucine enkephalin as lock mass.

TXRF measurements were performed on a Bruker S2 Picofox (Bruker, Berlin, Germany) with a molybdenum source. Europium(III) solutions of approximately 1000 ppm in milli-Q water were prepared and 500 µL of this solution was mixed with 500 µL of a 1000 ppm Chem-Lab gallium standard solution (1000 µg/mL, 2-5% HNO_3). 2 µL of this mixture with similar Eu(III)-Ga(III) concentrations was put on a Bruker AXS quartz glass sample plate for measurement.

Solutions were dispersed in a 180 W Bandelin Sonorex RK 510 H sonicator equipped with a thermostatic heating bath.

Absorption spectra were measured on a Varian Cary 5000 spectrophotometer on freshly prepared aqua solutions in quartz Suprasil cells (115F-QS) with an optical pathlength of 1 cm.

Emission spectra and luminescence decays of Eu(III) complexes were recorded on an Edinburgh Instruments FS980 steady state spectrofluorimeter. This instrument is equipped with a 450W xenon arc lamp, a high energy microsecond flashlamp mF900H and an extended red-sensitive photomultiplier (185–1010 nm, Hamamatsu R 2658P). All spectra are corrected for the instrumental functions. Luminescence decays were determined under ligand excitation (350 nm) monitoring emission of the $^5D_0 \rightarrow {}^7F_3$ transition for Eu(III) complexes. Luminescence decays were analyzed using Edinburgh software; lifetimes are averages of at least three measurements. Quantum yields were determined by a comparative method with a standard reference; estimated experimental errors for quantum yield determination ±10%. Rhodamine 101 (Sigma) in ethanol (Q=100%) was used as a standard for the complexes. Solutions with a concentration of about 10^{-5} M were prepared to obtain an optical density lower than 0.05 at the excitation wavelength.

Two photon excitation measurements were conducted using an inverted optical microscope (TiU, Nikon) equipped with a piezoelectric stage (Physik Instrument (PI) GmbH & Co.). A femtosecond laser (800 nm, 80 MHz, 120 fs, Maitai-HP, Spectra Physics) was reflected by a dichroic mirror (T750 spxrxt, Chroma) and was focused on the sample by an objective lens (PlanApo, x60, N.A. 0.98, Nikon). 2PE emission from 500 nm to 725 nm was collected by a spectrograph (iHR320, Horiba) and 2PE spectra were recorded by a cooled charge-coupled device (CCD) camera (DU920P, Andor). A shortpass cutoff filter (ET750SP-2P, Chroma) was placed in front of the spectrograph in order to reject the excitation laser light.

Relaxometry

^1H T_1 and T_2 measurements were performed at 310 K at 0.47, 1.41, 7.05, and 11.75 T on a Minispec mq-20, mq-60, Avance-300 and Avance-500 from Bruker, respectively. T_1 were measured using the inversion-recovery sequence and T_2 were obtained using CMPG sequence. The echo time was set to 1 ms. The diamagnetic contribution was the contribution of pure water.

DLS measurements

Dynamic light scattering was performed at room temperature with a BIC multiangle laser light-scattering system with a 90° scattering angle (Brookhaven Instruments Corporation, Holtsville, USA). The intensity weighted micellar diameter was measured on 0.01 wt% diluted suspensions in Milli-Q water, sonicated for 15 mins, passed through a 200 nm PTFE filter before analysis and calculated by a non-negatively constrained least-squares (multiple pass) routine.

Synthesis

DTPA-BC_{10}coumarin was synthesized as previously reported.[43]

DTPA-BC10Coumarinamide: ^1H NMR (300 MHz, DMSO, 25 °C, TMS) δ = 0.84 (t, 6 H), 1.24 (br, 28H), 1.52 (m, 4 H), 2.29 (br, 8 H), 3.30 (m, 4 H), 3.48 (m, 10 H), 7.23, 7.26 (d, 2 H), 8.21, 8.22, 8.24, 8.25 (dd, 2 H), 8.64, 8.65 (d, 2 H), 9.12 (t, 2 H), 10.98 ppm (s, 2 H). ^{13}C NMR (100 MHz, pyridine d-5, 25 °C, TMS) δ = 14.41, 22.56, 26.91, 29.17, 29.21, 29.37, 29.44, 29.46, 31.77, 40.31 (under solvent), 50.50, 51.19, 52.19, 52.86, 55.33, 116.63, 118.52, 119.42, 119.54, 126.17, 136.1, 147.49, 150.06, 160.79, 161.25, 170.03, 173.03, 173.4 ppm. ESI-MS (+ve mode): *m/z*: calcd 1046.6 $[M+H]^+$, found 1046.5 $[M+H]^+$.

DOTA-BC_{10}coumarin was synthesized as reported in a previous procedure by modifying the chromophore used.[29, 31]

DOTA-BC_{10}Coumarinamide: ^1H NMR (300 MHz, pyridine d-5, 25 °C, TMS) δ = 0.86 (t, 6 H), 1.22 (br, 28 H), 1.34 (m, 4 H), 1.63 (m, 4 H), 3.01-3.97 (br, DOTA 16 H), 3.58 (m, 4 H), 7.26, 7.29 (d, 2 H), 8.17, 8.19, 8.21, 8.24 (dd, 2 H), 8.66, 8.68 (d, 2 H), 9.10 (s, 2 H), 9.14 ppm (t, 2 H). ^{13}C NMR (100 MHz, pyridine d-5, 25 °C, TMS) δ = 14.13, 22.79, 27.22, 29.46, 29.72, 31.96, 39.98, 45.37, 50.02, 50.85, 54.08, 55.89, 62.93, 113.60, 116.54, 119.01, 119.49, 119.93, 122.38, 126.47, 147.99, 161.63, 161.96, 169.10, 174.42 ppm. ESI-MS (+ve mode): *m/z*: calcd 1057.6 $[M+H]^+$, found 1057.5 $[M+H]^+$.

Lanthanide(III) complexes

The ligands were coordinated to Ln(III) ions using previously reported procedures from 100 mg of free ligand in pyridine.[29, 31, 43]

Tb(III)-DOTA-BC_{10}Coumarinamide: Yield: 0.092 g, 80%; IR: ῡmax = 1563 (COO- asym. stretch), 1488 (amide II), 1435 cm^{-1} (COOsym. stretch); ESI-MS (-ve mode): *m/z*: calcd 1212.5 $[M-H]^-$, found 1211.5 $[M-H]^-$, 1246.6 $[M+Cl]^-$. HRMS (+ve mode): *m/z*: calcd 1214.5066 $[M+H]^+$, found 1214.5084 $[M+H]^+$. The complex decomposes above 300 °C.

Dy(III)-DOTA-BC_{10}Coumarinamide: Yield: 0.085 g, 74%; IR: ῡmax = 1562 (COO- asym. stretch), 1490 (amide II), 1436 cm^{-1} (COOsym. stretch); ESI-MS (-ve mode): *m/z*: calcd 1217.5 $[M-H]^-$, found 1216.4 $[M-H]^-$, 1252.5 $[M+Cl]^-$. HRMS (+ve mode): *m/z*: calcd 1219.5104 $[M+H]^+$, found 1219.5060 $[M+H]^+$. The complex decomposes above 300 °C.

Ho(III)-DOTA-BC_{10}Coumarinamide: Yield: 0.081 g, 70%; IR: ῡmax = 1563 (COO- asym. stretch), 1488 (amide II), 1437 cm^{-1} (COOsym.

View Article Online
DOI: 10.1039/C8DT01227J

stretch); ESI-MS (-ve mode): *m/z*: calcd 1218.5 $[M-H]^-$, found 1217.4 $[M-H]^-$, 1252.6 $[M+Cl]^-$. HRMS (+ve mode): *m/z*: calcd 1220.5115 $[M+H]^+$, found 1220.5106 $[M+H]^+$. The complex decomposes above 300 °C.

Eu(III)-DTPA-BC$_{10}$Coumarinamide: Yield: 0.063 g, 55%; IR: ῡmax = 1562 (COO- asym. stretch), 1489 (amide II), 1437 cm^{-1} (COOsym. stretch); ESI-MS (+ve mode): *m/z*: calcd 1196.4 $[M+H]^+$, found 1196.5 $[M+H]^+$. HRMS (+ve mode): *m/z*: calcd 1196.4422 $[M+H]^+$, found 1196.4435 $[M+H]^+$. The complex decomposes above 300 °C.

Preparation of micelles

1,2-Dipalmitoyl-sn-glycero-3-phosphocholine (DPPC, 80 mg, 0.109 mmol, 12 equiv.) and the amphiphilic complex (10 mg, ±0.091 mmol, 1 equiv.) were dissolved in a 1:1 chloroform/methanol solution (2 mL). After evaporation of the solvents in from flask with septum and needle fitted in a vacuum oven at 50 °C, a thin film was obtained which was rehydrated with hot water (2 mL, 70 °C). To improve the solubility, the suspension was sonicated in a 180 W sonicator with a thermostatic bath at 65 °C for 15 min. Polyoxyethylene sorbitan monooleate or Tween 80® (77 mg, 0.06 mmol, 6.5 equiv.) was added as a surfactant followed by another 15 min of sonication to fulfil the process of micelle formation. Water was evaporated in a flask with septum and needle fitted in a vacuum oven overnight at 50 °C leaving a thin film. A small amount of sample was removed for DLS measurements. For preparation of samples for relaxometry measurements, the thin film was rehydrated with Milli-Q water (1 mL), sonicated for 15 mins and passed through a 200 nm PTFE filter. The concentration of lanthanide(III) was analysed by TXRF before relaxometric measurements.

Notes and references

1 P. Caravan, J. J. Ellison, T. J. McMurry and R. B. Lauffer, *Chem. Rev.*, 1999, **99**, 2293-2352.
2 E. Debroye and T. N. Parac-Vogt, *Chem. Soc. Rev.*, 2014, **43**, 8178-8192.
3 A. Louie, *Chem. Rev.*, 2010, **110**, 3146-3195.
4 L. Frullano and T. J. Meade, *J. Biol. Inorg. Chem.*, 2007, **12**, 939-949.
5 D. Jańczewski, Y. Zhang, G. K. Das, D. K. Yi, P. Padmanabhan, K. K. Bhakoo, T. T. Y. Tan and S. T. Selvan, *Microsc. Res. Tech.*, 2011, **74**, 568-576.
6 J. C. Hebden, S. R. Arridge and D. T. Delpy, *Phys. Med. Biol.*, 1997, **5**, 825-840.
7 R. S. Balaban and V. A. Hampshire, *ILAR Journal*, 2001, **42**, 248-262.
8 J.-C. G. Bünzli, *J. Lumin.*, 2016, **170**, 866-878.
9 P. Caravan, *Chem. Soc. Rev.*, 2006, **35**, 512-523.
10 H. Dong, S.-R. Du, X.-Y. Zheng, G.-M. Lyu, L.-D. Sun, L.-D. Li, P.-Z. Zhang, C. Zhang and C.-H. Yan, *Chem. Rev.*, 2015, **115**, 10725-10815.
11 F. Wang and X. Liu, *Chem. Soc. Rev.*, 2009, **38**, 976-989.
12 E. Debroye, G. Dehaen, S. V. Eliseeva, S. Laurent, L. Vander Elst, R. N. Muller, K. Binnemans and T. N. Parac-Vogt, *Dalton Trans.*, 2012, **41**, 10549-10556.
13 G. Dehaen, S. V. Eliseeva, K. Kimpe, S. Laurent, L. Vander Elst, R. N. Muller, W. Dehaen, K. Binnemans and T. N. Parac-Vogt, *Chem. Eur. J.*, 2012, **18**, 293-302.
14 G. Dehaen, S. V. Eliseeva, P. Verwilst, S. Laurent, L. Vander Elst, R. N. Muller, W. Deborggraeve, K. Binnemans and T. N. Parac-Vogt, *Inorg. Chem.*, 2012, **51**, 8775-8783.
15 S. Carron, B. Maarten, L. Vander Elst, S. Laurent, T. Verbiest and T. N. Parac-Vogt, *Chem. Eur. J.*, 2016, **22**, 4521-4527.
16 G. Kandasamy, S. Surendran, A. Chakrabarty, S. N. Kale and D. Maity, *RSC Adv.*, 2016, **6**, 99948.
17 M. S. Moorthy, Y. Oh, S. Bharathiraja, P. Manivasagan, T. Rajarathinam, B. Jang, T. T. V. Phan, H. Jang and J. Oh, *RSC Adv.*, 2016, **6**, 110444-110453.
18 Q. Wang, C. Zhang, F. Guo, Z. Li, Y. Liu and Z. Su, *Bioconjugate Chem.*, 2017, **28**, 2841-2848.
19 M. Cano, R. Núñez-Lozano, R. Lumbreras, V. González-Rodríguez, A. Delgado-García, J. M. Jiménez-Hoyuela and G. d. l. Cueva-Méndez, *Nanoscale*, 2017, **9**.
20 A. Gautam and F. C. J. M. v. Veggel, *J. Mater. Chem. B*, 2013, **1**, 5186.
21 S. Carron, Q. Y. Li, L. Vander Elst, R. N. Muller, T. N. Parac-Vogt and J. A. Capobianco, *Dalton Trans.*, 2015, **44**, 11331.
22 S. Biju, M. Harris, L. Vander Elst, M. Wolberg, C. Kirschhock and T. N. Parac-Vogt, *RSC Adv.*, 2016, **6**, 61443-61448.
23 A. J. L. Villaraza, A. Bumb and M. W. Briechbiel, *Chem. Rev.*, 2010, **110**, 2921-2959.
24 P. Lebdušková, J. Kotek, P. Hermann, L. Vander Elst, R. N. Muller, I. Lukeš and J. A. Peters, *Bioconjugate. Chem.*, 2004, **15**.
25 C.-H. Huang, K. Nwe, A. A. Zaki, M. W. Brechbiel and A. Tsourkas, *ACS Nano*, 2012, **6**, 9416-9424.
26 Y. Li, M. Beija, S. Laurent, L. Vander Elst, R. N. Muller, H. T. T. Duong, A. B. Lowe, T. P. Davis and C. Boyer, *Macromolecules*, 2012, **45**, 4196-4204.
27 E. Debroye, S. Laurent, L. Vander Elst, R. N. Muller and T. N. Parac-Vogt, *Chem. Eur. J.*, 2013, **19**, 16019-16028.
28 E. Debroye, S. V. Eliseeva, S. Laurent, L. Vander Elst, R. N. Muller and T. N. Parac-Vogt, *Dalton Trans.*, 2014, **43**, 3589-3600.
29 M. Harris, S. Carron, L. Vander Elst, S. Laurent, R. N. Muller and T. N. Parac-Vogt, *Chem. Commun.*, 2015, **51**, 2984-2986.
30 M. Harris, S. Carron, L. Vander Elst and T. N. Parac-Vogt, *Eur. J. Inorg. Chem.*, 2015, 4572-4578.
31 M. Harris, L. Vander Elst, S. Laurent and T. N. Parac-Vogt, *Dalton Trans.*, 2016, **45**, 4791-4801.
32 J. W. Bulte, C. Wu, M. Brechbiel, R. A. Brooks, J. Vymazal, M. Holla and J. A. Frank, *Invest Radiol.*, 1998, **33**, 841-845.
33 T. N. Parac-Vogt, K. Kimpe, S. Laurent, C. Piérart, L. Vander Elst, R. N. Muller and K. Binnemans, *Eur. J. Inorg. Chem.*, 2004, 3538-3543.
34 K. Kimpe, T. N. Parac-Vogt, S. Laurent, C. Pierart, L. Vander Elst, R. N. Muller and K. Binnemans, *Eur. J. Inorg. Chem.*, 2003, **16**, 3021-3027.
35 T. N. Parac-Vogt, K. Kimpe, S. Laurent, C. Pierart, L. Vander Elst, R. N. Muller and K. Binnemans, *Eur. Biophys. J.*, 2006, **35**, 136-144.
36 M. Norek and J. A. Peters, *Progress in Nuclear Magnetic Resonance Spectroscopy*, 2011, **59**, 64-82.
37 M. Bloemen, S. Vandendriessche, V. Goovaerts, W. Brullot, M. Vanbel, S. Carron, N. Geukens, T. Parac-Vogt and T. Verbiest, *Materials*, 2014, **7**, 1155-1164.

View Article Online
DOI: 10.1039/C8DT01227J

38 K. Kattel, C. R. Kim, W. Xu, T. J. Kim, J. W. Park, Y. Chang and G. H. Lee, *J. Nanosci. Nanotechnol.*, 2015, **15**, 7311-7316.
39 T. S. Atabaev, Y. C. Shin, S.-J. Song, D.-W. Han and N. H. Hong, *Nanomaterials*, 2017, **7**, 216.
40 G. A. Pereira, J. A. Peters, F. A. A. Paz, J. Rocha and C. F. G. C. Geraldes, *Inorg. Chem.*, 2010, **49**, 2969-2974.
41 G. Piszczek, B. P. Maliwal, I. Gryczynski, J. Dattelbaum and J. R. Lakowicz, *J. Fluoresc.*, 2001, **11**, 101.
42 F. S. Richardson, *Chem. Rev.*, 1982, **82**, 541-552.
43 M. Harris, H. D. Keersmaecker, L. Vander Elst, E. Debroye, Y. Fujita, H. Mizuno and T. N. Parac-Vogt, *Chem. Commun.*, 2016, **52**, 13385.
44 H. Onishi and K. Sekine, *Talanta*, 1972, **19**, 473-478.
45 W. H. Lim and M. J. Lawrence, *Phys. Chem. Chem. Phys.*, 2004, **6**, 1380-1387.
46 A. Beeby, I. M. Clarkson, R. S. Dickins, S. Faulkner, D. Parker, L. Royle, A. S. d. Sousa, J. A. G. Williams and M. Woods, *J. Chem. Soc., Perkin Trans. 2*, 1999, 493-504.
47 R. M. Supkowski and W. D. H. Jr., *Inorg. Chim. Acta*, 2002, **340**, 44-48.
48 Y. Chen, R. Guan, C. Zhang, J. Huang, L. Ji and H. Chao, *Coord. Chem. Rev.*, 2016, **310**, 16-40.
49 T. Nemoto, R. Kawakami, T. Hibi, K. Iijima and K. Otomo, *Microscopy*, 2015, **64**, 9-15.
50 I. Solomon, *Physical Review*, 1955, **99**, 559-565.
51 N. Bloembergen, *J. Chem. Phys.*, 1957, **27**, 572-573.
52 J. H. Freed, *J. Chem. Phys.*, 1978, **68**, 4034-4037.
53 G.-L. Law, T. A. Pham, J. Xu and K. N. Raymond, *Angew. Chem. Int. Ed.*, 2012, **51**, 2371-2374.
54 L. Vander Elst, A. Roch, P. Gillis, S. Laurent, F. Botteman, J. W. M. Bulte and R. N. Muller, *Magn. Reson. Med.*, 2002, **47**, 1121-1130.
55 I. Bertini, F. Capozzi, C. Luchinat, G. Nicastro and Z. Xia, *J. Phys. Chem.*, 1992, **97**, 6351-6354.

View Article Online
DOI: 10.1039/C8DT01227J

Table of Contents Entry

Amphiphilic lanthanide(III) complexes self-assemble into monodisperse micelles with favourable properties for optical and high field magnetic resonance imaging